Strongly correlated superconductivity arising in a pseudogap metal

Marco Schiró,[1] Massimo Capone,[2,3] Michele Fabrizio,[1,4] and Claudio Castellani[2]
[1]*International School for Advanced Studies (SISSA), and CRS Democritos, CNR-INFM, Via Beirut 2-4, I-34014 Trieste, Italy*
[2]*SMC, CNR-INFM, and Università di Roma "La Sapienza," Piazzale Aldo Moro 2, I-00185 Roma, Italy*
[3]*Istituto dei Sistemi Complessi, CNR, Via dei Taurini 19, I-00185 Roma, Italy*
[4]*The Abdus Salam International Centre for Theoretical Physics (ICTP), P. O. Box 586, I-34014 Trieste, Italy*
(Received 23 January 2008; published 19 March 2008)

We solve by dynamical mean field theory a toy model that has a phase diagram strikingly similar to that of high-T_c superconductors: a bell-shaped superconducting region adjacent to the Mott insulator and a normal phase that evolves from a conventional Fermi liquid to a pseudogapped semimetal as the Mott transition is approached. Guided by the physics of the impurity model that is self-consistently solved within dynamical mean field theory, we introduce an analytical ansatz to model the dynamical behavior across the various phases which fits the numerical data very accurately. The ansatz is based on the assumption that the wave-function renormalization, which is very severe, especially in the pseudogap phase close to the Mott transition, is perfectly canceled by the vertex corrections in the Cooper pairing channel. A remarkable outcome is that a superconducting state can develop even from a pseudogapped normal state in which there are no low-energy quasiparticles. The overall physical scenario that emerges, although unraveled in a specific model and in an infinite-coordination Bethe lattice, can be interpreted in terms of arguments general enough to suggest that it can be realized in other correlated systems.

DOI: 10.1103/PhysRevB.77.104522 PACS number(s): 74.20.Mn, 71.27.+a, 71.30.+h, 71.10.Hf

I. INTRODUCTION

How high-temperature superconductivity can emerge out of a pseudogap metal is one of the standing puzzles posed by the cuprate superconductors. Indeed, one would expect that a pseudogapped metal is not ideal for superconductivity mainly for two reasons: the pseudogap reduces the density of states at the Fermi level and, more worrisome, it is likely to cut off the BCS singularity in the Cooper channel. As a consequence, a very strong pairing should be required to turn such an unconventional metal into a high-T_c superconductor. Many alternative proposals have been put forward to reconcile the existence of a pseudogap in the underdoped normal phase, which appears at a temperature T_*, with the occurrence of superconductivity (SC) below a critical temperature T_c that may become significantly smaller than T_* for deeply underdoped systems.

The simplest explanation is to associate the opening of a pseudogap with the existence of preformed Cooper pairs well above T_c.[1–5] This is compatible with the low dimensionality and the high critical temperature of the cuprates, which cooperate to enhance phase fluctuations of the order parameter, leading to a wide region where pairs are already formed yet the region lacks phase coherence. This scenario is experimentally supported by the strong diamagnetic response observed in an extended region above T_c.[6] However, even though this point of view is certainly reasonable close to T_c, its application close to the pseudogap temperature scale T_* and for small doping x is definitely more questionable. It is indeed well established that, while T_* increases monotonically as the doping $x \to 0$, both T_c and the superfluid density vanish. Within the preformed-pair picture, this would correspond to very strong coupling leading to localized pairs in real space, which can hardly be reconciled with the momentum-space nodal structure of the pseudogap observed by angle-resolved photoemission.[7]

A different point of view interprets the pseudogap as due primarily to a competing ordered phase[8–13] or arising from fluctuating competing orders among which d-wave superconductivity prevails below T_c (see Ref. 14 and references therein). Although compatible with much experimental evidence, these proposals pose, in our opinion, several theoretical questions. For instance, even if we assume that the pseudogap phase is a fluctuating mixture of different orders, we are still left with the question about the nature of the underlying normal phase unstable to all the above competing orders. A common belief is that the antiferromagnetic ground state of the undoped parent compounds[15] or another state very close in energy[16] must be interpreted as the *ancestor* phase that naturally evolves upon doping into a novel state of matter[14]—a fluctuating mixture of pseudogap phases—rather than into a *bona fide* normal metal that, below T_c, turns superconducting.

In this work, we do not intend to enter these controversial issues in the context of cuprates. Rather, we want to unravel in all its facets a similar phenomenology—the pseudogap normal phase which turns into a *high-temperature* superconductor—that we recently discovered by solving with dynamical mean field theory[17] (DMFT) a two-orbital Hubbard model inspired by fullerene superconductors.[18] We think that providing an exhaustive analysis of the pseudogap phenomenon in a strongly correlated model that can be exactly solved, albeit in an infinite-coordination lattice, may shed light on more realistic models for the cuprates, which are harder to deal with, both analytically and numerically. We are going to show that in this two-orbital model, akin to models for cuprates, superconductivity is the low-temperature winner among competing phases. In our case, two of these competing phases are homogeneous and symmetry invariant: a conventional Fermi-liquid metal and an intrinsic pseudogap phase, i.e., a single quantum phase with zero entropy at $T=0$. The connection between the supercon-

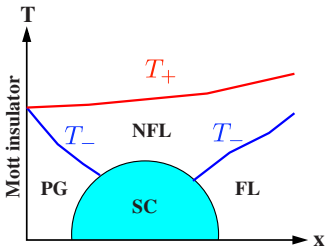

FIG. 1. (Color online) Sketch of the phase diagram of the model Eq. (1). x is a parameter that measures the deviation from the Mott insulator. FL, NFL, SC, and PG stand for normal Fermi-liquid, non-Fermi-liquid, superconducting, and normal pseudogap phases, respectively. T_- and T_+ are crossover lines; see the text.

ducting and the intrinsic pseudogap phases is intriguing, as the latter proves to be a fertile ground for superconductivity. The analysis of the self-energy in the superconducting phase reveals that the onset of superconductivity gives rise to much more coherent excitations than in the normal pseudogap state, where there are no quasiparticles and the self-energy diverges at low frequency. The way in which this singularity is regularized in the superconducting phase bears strong similarities to the effect of nonmagnetic impurities in an s-wave superconductor, where the processes leading to anomalies in the normal phase do not cut off the superconducting instability, or, in other words, they are *non-pair-breaking*. Despite the regularization of the low-frequency anomalies, where the superconducting gap develops, our correlated superconductor still presents the pseudogap energy scale at high frequency, and these two scales have opposite behavior as the doping goes to zero.

Although we are going to review in some detail the model and its properties in the following sections, we think is worth anticipating here some of the main results. In Fig. 1 we sketch the phase diagram of the model.[18] On the x axis we plot a parameter that controls the distance from a Mott insulating phase, like doping or pressure. The acronyms FL, NFL, SC, and PG stand for normal Fermi-liquid, non-Fermi-liquid, superconducting, and normal pseudogap phases, respectively. The temperature scale T_- (two branches) identifies the crossovers from the FL and PG phases into the almost critical NFL region. The latter is not pseudogapped and it is characterized by incoherent single-particle excitations with dispersion and inverse lifetime controlled by a single scale T_+. The Mott transition occurs when $T_+=T_-$ on the pseudogap side of the superconducting region.

The phase diagram Fig. 1 bears striking similarities to that of cuprates, if we identify the T_- branch on the "underdoped" side with T_*. From a purely theoretical point of view, the diagram closely resembles the quantum-critical-point (QCP) scenario proposed in many contexts, including cuprates[8–10] and heavy-fermion compounds,[11–13] as well as the phase diagram of the t-J model for cuprates[14,19,20] within the resonating valence bond (RVB) framework.[16] We postpone a critical comparison with those to the ending section of the paper.

The paper is organized as follows. In Sec. II we introduce our model and approach. Section III is devoted to the DMFT phase diagram, while Sec. IV summarizes the information that we can obtain from the impurity model which corresponds to our lattice model through DMFT. Sections V and VI introduce modelizations of the self-energy in the normal and superconducting phases, respectively. Finally, Sec. VII is dedicated to conclusions, with particular attention to the relation between our results and theoretical proposals for the cuprates.

II. THE MODEL

The model that we study is a two-orbital Hubbard model with the Hamiltonian

$$\mathcal{H} = -\sum_{ij}\sum_{a=1}^{2}\sum_{\sigma} t_{ij}(c^{\dagger}_{i,a\sigma}c_{j,a\sigma} + \text{H.c.}) + \frac{U}{2}\sum_{i}(n_i - 2)^2 - 2J\sum_{i}(T^2_{i,x} + T^2_{i,y}), \tag{1}$$

where $c^{\dagger}_{i,a\sigma}$ and $c_{i,a\sigma}$ create and annihilate, respectively, one electron at site i in orbital $a=1,2$ with spin σ, $n_i=n_{i,1}+n_{i,2}$ is the on-site occupation number, where $n_{i,a}=\Sigma_{\sigma}c^{\dagger}_{i,a\sigma}c_{i,a\sigma}$, and, finally,

$$T_{i,\alpha} = \frac{1}{2}\sum_{a,b=1}^{2}\sum_{\sigma} c^{\dagger}_{i,a\sigma}\tau^{\alpha}_{ab}c_{i,b\sigma} \tag{2}$$

are orbital pseudospin-1/2 operators, τ^{α} ($\alpha=x,y,z$) being the Pauli matrices. We assume hereafter that the exchange constant J is positive, and hence favors low-spin atomic configurations. This model was introduced in Ref. 18 to mimic an $e\otimes E$ Jahn-Teller coupling to a local doubly degenerate phonon mode that prevails over the conventional Coulomb exchange. In this case, the Jahn-Teller coupling leads effectively to inverted Hund's rules, with the provision that the phonon frequency is high enough to neglect retardation effects. The original purpose was to study a simplified model that shared the same physics of alkali-metal-doped fullerene superconductors, where pairing is mediated by eight fivefold-degenerate local vibrational modes, $t\otimes H$ Jahn-Teller coupled to the threefold degenerate lowest occupied molecular orbital (LUMO) of C_{60}.[21–23] Apart from a constant term, the Hamiltonian (1) can be alternatively written as

$$\mathcal{H} = -\sum_{ij}\sum_{a=1}^{2}\sum_{\sigma} t_{ij}(c^{\dagger}_{i,a\sigma}c_{j,a\sigma} + \text{H.c.}) + \frac{U}{2}\sum_{i}\sum_{a=1}^{2}(n_{i,a} - 1)^2 + \sum_{i} J_{\perp}\mathbf{S}_{i,1}\cdot\mathbf{S}_{i,2} + Vn_{i,1}n_{i,2}, \tag{3}$$

with $J_{\perp}=4J$ and $V=U+J$, which also describes two Hubbard models labeled by the orbital index $a=1,2$, coupled by an antiferromagnetic exchange $J_{\perp}$ and by a strong repulsion V.

The interaction term proportional to J in (1) is easily shown to generate an attraction that leads to an order parameter of s-wave symmetry associated with the operator

$$\Delta_{\mathbf{k}} = c^{\dagger}_{\mathbf{k},1\uparrow}c^{\dagger}_{-\mathbf{k},2\downarrow} + c^{\dagger}_{-\mathbf{k},2\uparrow}c^{\dagger}_{\mathbf{k},1\downarrow}. \tag{4}$$

The bare scattering amplitude in this channel is $A=-2J$, and it would induce a superconducting instability in the absence

of Coulomb repulsion. The introduction of U weakens the attraction, leading to $A=-2J+U$. Therefore, at least in weak coupling, $U,J \ll W$ (W being the noninteracting bandwidth), one expects the model to describe a BCS superconductor for $U \leq 2J$, and a normal metal for larger repulsion. In principle, if the noninteracting Fermi surface accidentally has nesting, other weak-coupling instabilities like, e.g., magnetism can occur. In our calculation we did not consider such commensurate phases, because they are related to specific aspects of the lattice, and we want to focus on more basic and general properties. We note that the competition between attraction and repulsion, namely, between $J_\perp$ and V in (3), offers the opportunity to investigate how s-wave superconductivity can emerge at all in spite of strong correlations. This issue is not commonly touched in the context of cuprates, where the emphasis is mostly put on the appearance of d-wave superconductivity (whose order parameter exists on the bonds) in the presence of purely on-site repulsion, while longer-range contributions to the interaction are often ignored.[24]

Let us move now to the opposite limit of strong repulsion, $U \gg W$, and consider the half-filled case. In this limit the model is a Mott insulator, each site being occupied by two electrons that cannot move coherently. When $J=0$ the model maps onto an SU(4) Heisenberg model. If the hopping is restricted to nearest neighbors, the ground state of this model is dimerized in one dimension,[25] while in a two-dimensional square lattice it is still unclear whether it is a spin liquid or Néel ordered.[26,27] When the attraction is switched on and $J \gg W^2/U > 0$, the attractive interaction prevails and two electrons on each site i lock into the singlet state

$$\frac{1}{\sqrt{2}}(c^\dagger_{i,1\uparrow}c^\dagger_{i,2\downarrow} + c^\dagger_{i,2\uparrow}c^\dagger_{i,1\downarrow})|0\rangle, \tag{5}$$

stable to the weak intersite superexchange. In this case, the Mott insulator is nonmagnetic and translationally invariant—a local version of a valence-bond crystal—regardless of the structure of the hopping matrix element and the dimensionality and topology of the lattice. A sufficient degree of frustration, due to either the lattice topology or the hopping amplitudes t_{ij}, disfavors a magnetic state and makes it possible for this nonmagnetic phase to survive decreasing U/W down to the Mott transition, which is in turn pushed to a finite U_c when frustration eliminates nesting. When this happens, one should naively expect, as U/W is increased at fixed $J/W \ll 1$, first a very narrow BCS superconducting region for $0 \leq U \leq 2J$, followed by a normal metal, which eventually gives way to a nonmagnetic Mott insulator when $U \geq U_c \sim W$. Seemingly, doping the nonmagnetic Mott insulator at $U > U_c \gg J$ should bring a normal metal which, as doping increases, gets less and less correlated.

This naive expectation, based essentially on the value of the bare scattering amplitude $A=-2J+U$ in the singlet Cooper channel Eq. (4), turns out to be wrong at least in the two cases that have been so far considered: (i) an infinite-coordination Bethe lattice,[18] which is exactly solved by DMFT; (ii) a one-dimensional chain.[28] We will briefly mention the latter in the last section, while in what follows we concentrate mostly on the DMFT results for the Bethe lattice. In the following we first recall the basic ideas behind DMFT,[17] and our implementation.

DMFT extends the idea of the classical mean field to the quantum domain: a lattice model is approximately solved by solving the quantum problem of a single site subject to a "dynamical Weiss field" that describes the action of the rest of the lattice sites on the given site (assumed to be equivalent to any other). As in classical mean field theory, the mapping is exact only in infinite-coordination lattices. The effective action of the local degrees of freedom reads

$$S_{\text{eff}} = \int_0^\beta d\tau\, d\tau'\, c^\dagger_{0\alpha\sigma}(\tau)\mathcal{G}_0^{-1}(\tau-\tau')^{\alpha\beta}_{\sigma\sigma'}c_{0\beta\sigma'}(\tau') + S_0[c_{0\alpha\sigma}, c^\dagger_{0\alpha\sigma}], \tag{6}$$

where $\mathcal{G}_0^{-1}$ is the Weiss field, α and β are orbital indices, and σ and σ' are spin indices. S_0 is the local part of the action and contains all local interaction terms of the lattice Hamiltonian. The mean field scheme is closed by imposing between the Weiss field and the local Green's function $G(\tau-\tau')$, computed by the action (6), a self-consistency relation that contains the information about the original lattice model through the noninteracting density of states (DOS), For a Bethe lattice with nearest-neighbor hopping and bandwidth W, which we consider hereafter, the self-consistency reads

$$\mathcal{G}_0^{-1}(i\omega_n)^{\alpha\beta}_{\sigma\sigma'} = i\omega_n - E^{\alpha\beta}_{\sigma\sigma'} - \frac{W^2}{16}G(i\omega_n)^{\alpha\beta}_{\sigma\sigma'}, \tag{7}$$

where E is the matrix of the single-particle terms of the on-site Hamiltonian (chemical potential, magnetic field, hybridization) and $G(i\omega_n)$ is the Fourier transform of the local Green's function $G(\tau)^{\alpha\beta}_{\sigma\sigma'} = -\langle T_\tau c_{0\alpha\sigma}(\tau)c^\dagger_{0\beta\sigma'}(0)\rangle_{S_{eff}}$. Equations (6) and (7) can be viewed as a set of two coupled equations for G and $\mathcal{G}_0^{-1}$. In practice, one needs to solve (6) for a given choice of $\mathcal{G}_0^{-1}$ and obtaining G. Using (7) one finds a new value of $\mathcal{G}_0^{-1}$. The procedure is iterated until convergence is achieved. It is evident that the computation of G is the hard part of the calculation. An important observation is that the effective local theory can be represented as an impurity model whose hybridization function coincides with the dynamical Weiss field. In practice, a DMFT calculation amounts to solving an Anderson impurity model iteratively in order to self-consistently determine its hybridization function.

The solution of the impurity model requires either an approximate numerical method, or an "exact" numerical approach. In this work we use exact diagonalizaton at $T=0$,[29] which amounts to approximating the continuous bath of the impurity model by a discrete set of energy levels hybridized with the impurity. The method has been shown to converge exponentially as a function of the number N_b of bath levels. For example, $N_b=5$ already gives quite reliable results for the phase diagram and thermodynamic observables of a single-band Hubbard model. In this work we will use six bath levels for each orbital, which gives $N_b=12$ in total. An important aspect of the exact diagonalization method is the way in which the continuous bath is approximated. This is

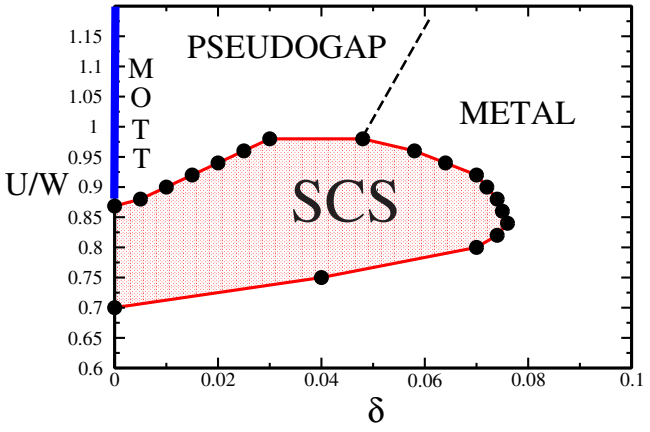

FIG. 2. (Color online) DMFT phase diagram of the model Eq. (1) as a function of U/W and doping δ.

implemented by minimizing a suitably chosen distance between two functions. The distance is typically computed on the imaginary axis on a Matsubara grid corresponding to an effective temperature $\tilde{\beta}$, which is not to be confused with the physical temperature, always set to $T=0$. In this work we typically use $\tilde{\beta}=400/W$, and define a distance that weights more low frequencies.[30] Specifically, we minimize

$$\chi = \sum_n \frac{|\mathcal{G}_0^{-1} - (\mathcal{G}_0^{-1})_{\text{discrete}}|}{\omega_n} \tag{8}$$

$(\mathcal{G}_0^{-1})_{\text{discrete}}$ being the discrete version of the Weiss field, with the sum extending up to a maximum frequency of order $4U$.

Finally, in order to describe the superconducting phase, the bath includes superconducting terms leading to a Weiss field with anomalous components. Consequently, the impurity Green's function has also an anomalous term $F_{\alpha\beta}(\tau) = -\langle T_\tau c_{\alpha\uparrow}(\tau) c_{\beta\downarrow}(0)\rangle$, which is used together with G to build the matrix $\hat{G}(i\omega_n)$ in the Nambu-Gor'kov formalism. Seemingly, one defines a matrix Weiss field with diagonal, $\mathcal{G}^0(i\omega_n)^{-1}$, and off-diagonal, $\mathcal{F}^0(i\omega_n)^{-1}$, components. The self-consistency condition (7) can be rewritten in the same formalism straightforwardly.

III. THE PHASE DIAGRAM IN A BETHE LATTICE

In Fig. 2 we show the DMFT phase diagram of model (1) at fixed $J=0.05\ W$ in a Bethe lattice as a function of doping and U/W around the Mott transition, $U_c \simeq 0.87\ W$.[18] The first remarkable thing to note is the appearance of superconductivity, denoted as SCS (for strongly correlated superconductivity, see below) in the figure, just around the Mott transition. The symmetry of the order parameter is that of Eq. (4). Superconductivity even extends for $U \gtrsim U_c$ within a finite doping interval and is preceded by a pseudogap metal and followed, at larger doping, by a more conventional normal metal; see Fig. 2. We emphasize that the discreteness of the spectra obtained in exact diagonalization does not allow us to unambiguously identify the pseudogap region, yet the results clearly show the evolution from one kind of normal state into the other, as already shown in Ref. 18.

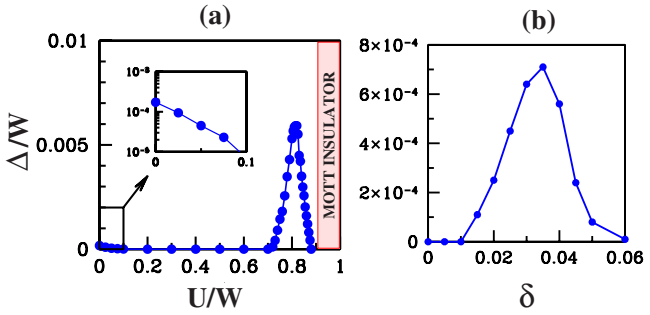

FIG. 3. (Color online) Superconducting gap at half filling as a function of U/W (a), and for $U=0.92\ W$ as a function of doping away from half filling (b). The inset in (a) shows the gap at weak U on an enlarged scale.

The strength of pairing is also surprising. In Fig. 3 we draw the values of the superconducting gap Δ at half filling as a function of U/W, Fig. 3(a), and at $U=0.92\ W$ as a function of doping, Fig. 3(b). In Fig. 3(a) we also show on a smaller scale the same quantity in the BCS-like region for small $U \leq 2J$. The latter is exponentially small, in agreement with the BCS estimate $\Delta \sim 0.5W \exp(-\pi W/8J) \sim 2\times 10^{-4} W$, almost two orders of magnitude smaller that the values attained in the superconducting region around the Mott insulator.

This superconducting phase that reemerges with strengthened pairing just before the Mott transition was named in Ref. 23 *strongly correlated superconductivity* to emphasize its peculiar properties with respect to conventional BCS superconductors. Indeed, in addition to the large value of the gap in spite of the tiny attraction $J=0.05\ W$, other features characterize SCS. In Fig. 4(a) we compare the values at half filling of the Drude weight [zero-frequency contribution to the optical conductivity $\sigma(\omega)$] in the SCS phase and in what could be regarded as the *normal phase*, namely, the metastable solution obtained within DMFT by preventing gauge symmetry breaking. We note that the onset of superconductivity is accompanied by an increase of Drude weight, unlike what happens in a BCS superconductor. Remarkably, while the SCS Drude weight vanishes only at the Mott transition, the weight of the normal solution vanishes for a smaller U when the zero-frequency spectral weight goes to zero, sug-

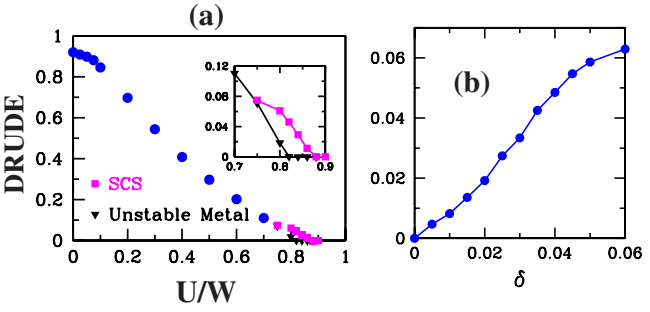

FIG. 4. (Color online) (a) Drude weight at half filling as a function of U/W. In the SCS region is also shown the Drude weight of the metastable normal solution, zoomed in the inset. (b) Drude weight at $U=0.92\ W$ as a function of doping.

gesting the opening of the pseudogap. This semiconducting normal phase is metastable at half filling, where the stable zero-temperature phase is superconducting, but it is stabilized away from half filling as shown in the phase diagram of Fig. 2. Here, doping seems to have the same effect as in semiconductors, leading to a Drude weight linearly increasing with the number of holes, reported in Fig. 4(b). The intrusion of SCS leads to a more pronounced increase of Drude weight which smoothly connects to the normal metal appearing for larger doping.

A. Fermi-liquid description

Since the stable metallic phases at small U/W at half filling, or at large doping away from half filling, do not show any particular anomaly, a Landau Fermi-liquid scenario is expected to be applicable in understanding how superconductivity can emerge in spite of the fact that the bare scattering amplitude in the Cooper channel is repulsive. The Fermi-liquid behavior is indeed confirmed by the regular self-energies calculated by DMFT. Within perturbation theory, the effect of interaction on the low-energy single-particle properties can be absorbed into the so-called wave-function renormalization or quasiparticle residue Z defined by

$$\frac{1}{Z} = 1 - \left(\frac{\partial \Sigma(i\omega_n, k_F)}{\partial i\omega_n} \right)_{\omega_n \to 0}, \tag{9}$$

where $\Sigma(i\omega_n, k_F)$ is the single-particle self-energy in Matsubara frequencies at the Fermi momentum, and by the reduction of the quasiparticle bandwidth $W \to W_* < W$,

$$\frac{W_*}{W} = Z\left[1 + \frac{1}{v_F^0} \left(\frac{\partial \Sigma(0,k)}{\partial k} \right)_{k=k_F} \right], \tag{10}$$

where v_F^0 is the bare Fermi velocity. Z can be regarded as the component of the total single-particle spectral weight that is carried by coherent quasiparticle excitations. In general $Z \leq W_*/W$, the equality holding only in infinite-coordination lattices where the self-energy is momentum independent, $\Sigma(i\omega_n, k) \equiv \Sigma(i\omega_n)$.[31]

Within Landau theory, considering a generic scattering channel with bare amplitude Λ, the renormalized value can be written as

$$\Lambda_* = Z^2 \Gamma_\Lambda \Lambda, \tag{11}$$

where Γ_Λ includes the so-called vertex corrections. Approaching an interaction-driven Mott transition, $U \to U_c$, the quasiparticle residue vanishes $Z \propto U_c - U \to 0$, but the behavior of Λ_* in different channels can be totally different due to the different relevance of vertex corrections. Physical intuition suggests that the proximity to a Mott transition affects primarily charge fluctuations, which are severely suppressed, but it does not equally influence the way in which the charge is distributed between different spin and orbital states. Indeed, the localization of the charge leads to the formation of local moments and reflects an enhancement of the spin and orbital responses. This suggests that, while vertex corrections in the spin- and orbital-density channels can compensate the vanishing Z, the same cancellation does not take place in the charge-density channel. Following this observation, we argued in Ref. 23 that the on-site repulsion U and exchange J undergo different renormalization as the Mott insulator is approached. In particular, since the exchange term J only controls the multiplet splitting at fixed charge, it is not affected by the approach to the Mott transition; hence $J \to J_* \simeq J$. On the contrary, the residual quasiparticle repulsion is substantially weakened near a Mott transition, since most correlation effects are already built into the small Z. On the basis of the DMFT behavior of the double occupancy in the single-band Hubbard model,[17] it was speculated in Ref. 23 that $U \to U_* \simeq ZU$. This assumption would result in the ansatz for the quasiparticle scattering amplitude in the Cooper channel 4

$$A = U - 2J \to A_* = U_* - 2J_* \simeq ZU - 2J. \tag{12}$$

Should Eq. (12) be correct, it would imply that A_*, which for small $U > 2J$ is repulsive in agreement with perturbation theory, must necessarily turn attractive sufficiently close to the Mott transition, where Z goes to zero. In Fig. 5 we show A_* given by Eq. (12) with Z extracted according to Eq. (9) from the normal-state DMFT solution. We note that this estimate for A_* changes from repulsive to attractive very close to the point where a stable superconducting solution is found, supporting the validity of (12). Moreover, the expression (12) provides an explanation for the large strength of pairing in the SCS phase in comparison with the BCS state. In fact, as $Z \to 0$, a regime in which $A_* \simeq -W_* = -ZW$ is eventually reached. Here the quasiparticles experience an attraction of the same order as their effective bandwidth. This intermediate regime, bridging between the weak-coupling BCS limit and the strong-coupling Bose regime, has been shown to be the optimal situation for superconductivity in purely attractive models.[32,33]

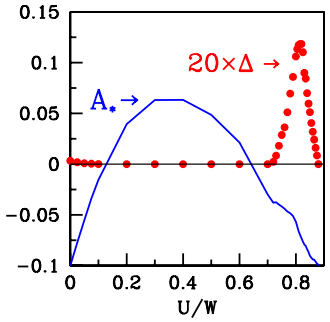

FIG. 5. (Color online) Ansatz for the scattering amplitude $A_* = ZU - 2J$ versus U/W using Z extracted from a normal DMFT solution. Also shown is the superconducting gap multiplied by a factor of 20 for graphic convenience.

According to the above Fermi-liquid arguments, superconductivity reemerges before the Mott transition because our Hamiltonian contains a pairing mechanism whose only role is to favor the singlet configuration (5) whenever two electrons are on the same site. For this reason pairing is strengthened rather than weakened as Mott localization is approached. A similar phenomenon is not expected to occur

if pairing is mediated by a charge-charge attraction, which obviously conflicts with the Coulomb repulsion. Notice that in the present context the origin of J (purely electronic generated, e.g., by superexchange, or driven by coupling with Jahn-Teller phonons as in fullerenes[21]) is not important, the only relevant point being that it does not compete with U.

IV. INSIGHTS FROM THE IMPURITY MODEL

Although Fermi-liquid theory can be rather safely invoked to explain the emergence of superconductivity from the correlated metal, it has to be eventually abandoned in the region of coupling which precedes the Mott transition, where, as we discussed, superconductivity emerges out of a pseudogap normal phase. This demands an alternative description able to account for both the Fermi-liquid and non-Fermi-liquid regimes.

As we introduced in Sec. II, DMFT establishes a correspondence between a lattice model and an impurity model. The equivalence between the two models is enforced by a self-consistency condition which contains the information about the original lattice. The role of the DMFT self-consistency is absolutely nontrivial: for instance it makes the impurity Kondo temperature T_K vanish at a finite value of the interaction which signals the Mott transition in the lattice model, since T_K coincides with the renormalized bandwidth $W_*=Z\ W$. However, important insights can be gained by the analysis of the impurity model alone, without imposing the self-consistency.

The Hamiltonian of the impurity model corresponding to (1) is

$$\mathcal{H} = -\sum_{\mathbf{k}}\sum_{a=1}^{2}\sum_{\sigma}\epsilon_{\mathbf{k}}c^{\dagger}_{\mathbf{k},a\sigma}c_{\mathbf{k},a\sigma} + (V_{\mathbf{k}}c^{\dagger}_{\mathbf{k},a\sigma}d_{a\sigma} + \text{H.c.}) + \frac{U}{2}(n_d-2)^2 - 2J(T_x^2+T_y^2), \tag{13}$$

where $c^{\dagger}_{\mathbf{k},a\sigma}$ and $c_{\mathbf{k},a\sigma}$ are auxiliary fermionic degrees of freedom introduced to describe the Weiss field, while $d^{\dagger}_{a\sigma}$, $d_{a\sigma}$, n_d, and $T_{x(y)(z)}$ are the same operators defined above, but specialized to the impurity site. The physics of the model is controlled by three energy scales: U, J and the so-called hybridization width Γ defined through

$$\Gamma = \pi\sum_{\mathbf{k}}|V_{\mathbf{k}}|^2\delta(\epsilon_{\mathbf{k}}). \tag{14}$$

The Hamiltonian (13) has been recently studied in Refs. 34–36 by means of numerical renormalization group (NRG) for a constant hybridization function.[37,38] It has been found that, as a function of U at fixed Γ and $J\ll\Gamma$, a quantum phase transition takes place at $U=U_*$, an interaction value that corresponds to a Kondo temperature $T_K^*\simeq J$. For $U<U_*$, i.e., $T_K>T_K^*$, perfect Kondo screening takes place. On the contrary, when $U>U_*$, $T_K<T_K^*$, the impurity locks into the singlet configuration

$$\frac{1}{\sqrt{2}}(d^{\dagger}_{1\uparrow}d^{\dagger}_{2\downarrow} + d^{\dagger}_{2\uparrow}d^{\dagger}_{1\downarrow})|0\rangle, \tag{15}$$

which does not require any Kondo screening. The critical point that separates the two phases is similar to that found in the two impurity Kondo model.[39,40] Moreover the critical point exists also away from particle-hole symmetry, and, remarkably, it can be accessed even for $U>U_*$ by changing the density away from half filling.[35] The single-particle spectral function displays an interesting evolution across the transition.[35] In the Kondo screened phase, the low-frequency DOS is characterized by a broad resonance around the Fermi level, on top of which a narrow Kondo peak develops. The latter shrinks continuously as the critical point is approached, while the broad resonance stays unaffected, as well as the high-energy Hubbard bands surrounding the low-energy features. At the critical point, the Kondo peak disappears, leaving behind only the broad resonance. In the unscreened phase, a narrow pseudogap appears inside the broad resonance, whose width grows on moving away from the critical point. This pseudogap is gradually filled away from particle-hole symmetry, although, as mentioned, the critical point still exists. This behavior has been parametrized[35] by the following ansatz for the low-energy DOS at particle-hole symmetry:

$$\rho(\epsilon) = \frac{1}{\pi\Gamma}\left(\frac{T_+^2}{\epsilon^2+T_+^2} \pm \frac{T_-^2}{\epsilon^2+T_-^2}\right), \tag{16}$$

where the plus and minus signs refer to the screened and unscreened phases, respectively. The energy scale $T_+ \sim \max(T_K,J)$ measures the width of the broad resonance, while $T_- \propto |U-U_*|^2$ controls the deviation from the fixed point and sets the width of the Kondo peak in the screened phase and of the pseudogap in the unscreened one. This model DOS defines a self-energy that was shown to fit perfectly well the numerical data for the impurity model.[35] In particular, the self-energy at small Matsubara frequencies is Fermi-liquid-like in the Kondo screened phase, $\Sigma(i\omega_n) \propto -i\omega_n$, is finite and imaginary at the critical point, $\Sigma(i\omega_n) = -i\Gamma$, and diverges in the unscreened phase, $\Sigma(i\omega_n) \propto 1/i\omega_n$.

The critical point is unstable in several symmetry-breaking channels,[34,40] including the magnetic channel

$$\mathbf{S}_1 - \mathbf{S}_2, \tag{17}$$

the Cooper channel Eq. (4), and the hybridization channels

$$\sum_{\sigma} d^{\dagger}_{1\sigma}d_{2\sigma}, \quad \sum_{\sigma} d^{\dagger}_{2\sigma}d_{1\sigma}, \tag{18}$$

that break the O(2) orbital symmetry. All these channels are degenerate at the critical point, where the model has an enlarged SO(7) symmetry.[40] When the impurity model contains explicitly a symmetry-breaking term that couples to one of the unstable channels, the critical point is washed out and the phase transition between the Kondo and the local singlet phase turns into a sharp crossover.[35,36] In the meantime, the relevant perturbation cuts off the non-Fermi-liquid singularities of the self-energy both at the critical point and in the

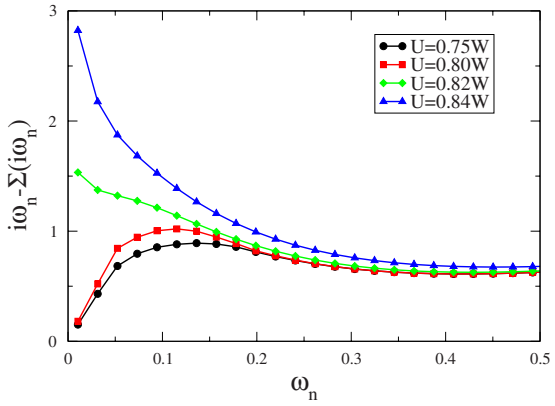

FIG. 6. (Color online) $i\omega_n - \Sigma(i\omega_n)$ versus $\omega_n > 0$ for different values of U/W, as obtained by DMFT preventing superconductivity.

unscreened phase, so that, at sufficiently low frequency, $\Sigma(i\omega_n) \propto -i\omega_n$ is always recovered.[36]

Since the Kondo temperature T_K has to vanish as the Mott transition is approached, the effective impurity model must encounter the critical point, $T_K \simeq J$, before the Mott point is reached. In Ref. 34 it has been speculated that, once a full DMFT calculation is carried on, the instabilities associated with the impurity critical point lead because of the self-consistency condition to a spontaneous symmetry breaking in a whole region around the critical point along one of the instability channels. These are the particle-hole channels (17) and (18), which correspond to magnetic and orbital ordering, respectively, and the particle-particle channel (4) which implies superconductivity. This prediction is perfectly compatible with the DMFT phase diagram, Fig. 2. We note that particle-hole instabilities usually require nesting or other band-structure singularities that only accidentally occur, while the Cooper singularity is more ubiquitous. For this reason, in Ref. 18 we only searched for a superconducting instability, even though the Bethe lattice with nearest-neighbor hopping has nesting at half filling.

V. MODELING THE DYNAMICS IN THE NORMAL PHASES

The analysis of the previous section shows that the critical point of the impurity model is expected to be always preempted by broken-symmetry phases in the lattice model treated within DMFT. Nonetheless, it is plausible that the critical point corresponds to a metastable phase, just as a normal metal is a metastable phase in the presence of attraction. Following this idea, we have solved the model (1), forcing the DMFT self-consistency not to break any symmetry. The behavior of the self-energy that we obtain (see Fig. 6) closely recalls that of the impurity model with constant bath (i.e., without self-consistency) that we just discussed. This confirms that the impurity critical point corresponds to a metastable phase in the lattice model and suggests that the same parametrization Eq. (16) may work in the lattice as well. Therefore we have assumed for the low-frequency local Green's function the following expression, valid in a Bethe lattice (all energies will be expressed in units of the bandwidth $W=1$):

$$\mathcal{G}(i\omega_n) = \frac{1}{2}\left[\mathcal{G}_0\left(\frac{i\omega_n}{T_+}\right) \pm \mathcal{G}_0\left(\frac{i\omega_n}{T_-}\right)\right], \tag{19}$$

where the $\pm$ sign, T_+, and T_- have the same meaning as in Eq. (16), while

$$\mathcal{G}_0(i\omega_n) = 8i\left(\omega_n - \mathrm{sgn}(\omega_n)\sqrt{\omega_n^2 + \frac{1}{4}}\right) \tag{20}$$

is the noninteracting local Green's function. The ansatz (19) for the Green's function corresponds to an ansatz for the self-energy which, through the DMFT self-consistency equation, becomes

$$\Sigma(i\omega_n) = i\omega_n - \frac{1}{16}\mathcal{G}(i\omega_n) - \mathcal{G}(i\omega_n)^{-1}. \tag{21}$$

In the Fermi-liquid region, where the plus sign has to be used in (19) and $T_- \neq 0$, the low-frequency self-energy is

$$\Sigma(i\omega_n) \simeq i\omega_n - i\frac{\omega_n}{2}\left(\frac{1}{T_+} + \frac{1}{T_-}\right) + i\frac{\omega_n^2}{4}\left(\frac{1}{T_+} - \frac{1}{T_-}\right)^2 \mathrm{sgn}(\omega_n), \tag{22}$$

corresponding to a regular Fermi-liquid behavior with quasiparticle residue

$$Z = 2\frac{T_+T_-}{T_+ + T_-}. \tag{23}$$

At the critical point ($T_-=0$), or for frequencies $T_- \ll \omega_n \ll T_+$, the self-energy becomes

$$\Sigma(i\omega_n) \simeq i\omega_n - i\frac{3}{8}\mathrm{sgn}(\omega_n) - i\frac{5\omega_n}{4T_+} - i\frac{3}{4}\left(\frac{\omega_n}{T_+}\right)^2 \mathrm{sgn}(\omega_n). \tag{24}$$

$\Sigma(i\omega_n)$ has a finite and sizable imaginary part, implying a non-Fermi-liquid behavior. The deviations from conventional Fermi-liquid behavior become even more pronounced in the unscreened phase, where $T_- \neq 0$ and the minus sign has to be used in (19). Here we obtain

$$\Sigma(i\omega_n) \simeq i\omega_n - \frac{i}{4\omega_n}\frac{T_+T_-}{T_+ - T_-} - \frac{i}{4}\frac{T_+ + T_-}{T_+ - T_-}\mathrm{sgn}(\omega_n) - i\frac{\omega_n}{T_+ - T_-}. \tag{25}$$

The divergence of $\Sigma(i\omega_n)$ for small ω_n leads to a pseudogap in the DOS, whose behavior at small energy is

$$\rho(\epsilon) \simeq 4\left(\frac{1}{T_-^2} - \frac{1}{T_+^2}\right)\epsilon^2. \tag{26}$$

We can check the validity of our ansatz by simply comparing it with the actual DMFT results obtained using exact diagonalization. Fitting these data with (19), we find a very good agreement, and we can extract the parameters T_+ and T_-. The behavior of the best-fit values of T_+ and T_- is drawn in Fig. 7 and supports our ansatz, and consequently the relevance of

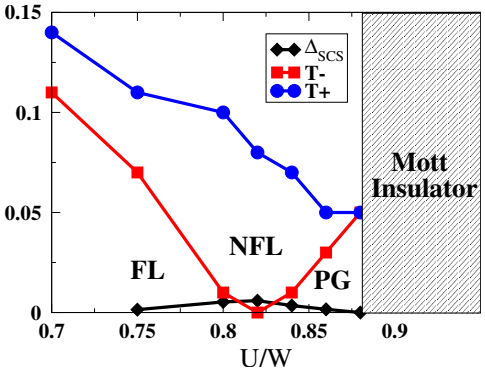

FIG. 7. (Color online) Fitting parameters T_+ and T_- of the DMFT normal self-energy with the expression Eq. (21) using for the impurity Green's function Eq. (19). We also draw the DMFT superconducting gap when gauge symmetry breaking is allowed.

the impurity critical point for the lattice model. In the same figure we report the superconducting gap obtained in DMFT allowing for gauge-symmetry breaking.

Two things are worth noting in this figure. First, the vanishing of T_- at $U \simeq 0.82\ W$, namely, the location of the *metastable* critical point, corresponds to the maximum of the superconducting gap once gauge symmetry breaking is allowed, in accordance with the prediction based on the analysis of the impurity model.[34] At the metastable critical point, the only remaining energy scale is T_+, which therefore determines the maximum value of the superconducting gap Δ. Second, the Mott transition occurs within the pseudogap region when $T_-=T_+$. In other words, the pseudogap gradually widens as U increases from the $T_-=0$ point and, at the same time, the total spectral weight of the low-energy part, given by (T_+-T_-) according to Eq. (19), diminishes until it disappears, when $T_-=T_+$.

Although we solved the DMFT at zero temperature, we believe that the $T=0$ energy scales will at least approximately determine the finite-temperature behavior of the model. We can therefore speculate that the energy scales T_+, T_-, and Δ will be reflected in analogous temperature scales, leading to the scenario drawn in Fig. 1 and discussed in the Introduction. In this perspective, even though the critical region around $T_-=0$ is not stable at $T=0$, and in fact in our calculation is replaced by superconductivity, it should become accessible by raising the temperature T when $T_+ > T > \max(T_-, T_c)$, denoted as NFL (non-Fermi-liquid) in the figure. If we follow a path in the T-U space that avoids the bell-shaped superconducting region, we must find a crossover from a correlated Fermi-liquid phase to a pseudogap state passing through the NFL region.

Finally, the region above T_+ has a simple interpretation in the impurity model, where it corresponds to the local moment regime above the Kondo temperature. In the lattice model, it presumably translates into a phase with very poor lattice coherence, although its precise properties are difficult to foresee in the absence of actual finite-T calculations.

VI. MODELING THE DYNAMICS IN THE SUPERCONDUCTING PHASE

An important result for the impurity model is that, as soon as one of the relevant symmetry-breaking perturbations is introduced, such as, e.g., the hybridization (18), suddenly the non-Fermi-liquid behavior of the self-energy is replaced by a standard Fermi-liquid one. In this case the low-frequency self-energy at the critical point changes from an imaginary constant to a conventional linearly vanishing function.[36] We can therefore expect a similar regularization to occur as soon as superconductivity is allowed in the lattice model. This expectation is closely reminiscent of the mechanism taking place when s-wave superconductivity is established in a disordered metal. Here scattering off impurities makes the quasiparticle lifetime $1/\tau$ finite, which means that the normal-state self-energy is finite and imaginary at zero frequency, just as in the above discussed non-Fermi-liquid phase. Following Abrikosov, Gor'kov, and Dzyaloshinskii,[41] we write the self-energy as a 2×2 matrix whose diagonal entry Σ_{11} is the normal component, and whose off-diagonal entry Σ_{12} is the anomalous (superconducting) contribution. We define the function $\eta(i\omega_n)$ in the normal phase according to

$$i\omega_n - \Sigma_{11}(i\omega_n) = i\omega_n + \frac{i}{2\tau}\mathrm{sgn}(\omega_n) \equiv i\omega_n \eta(i\omega_n). \quad (27)$$

The onset of superconductivity regularizes this normal-state anomaly, giving rise to a normal self-energy Σ_{11} linear below a low-energy scale Δ and, at the same time, the anomalous self-energy Σ_{12} gets strongly enhanced with respect to that of a clean superconductor, namely,[41]

$$i\omega_n - \Sigma_{11}(i\omega_n) = i\omega_n \eta(i\sqrt{\omega_n^2+\Delta^2}), \quad (28)$$

$$\Sigma_{12}(i\omega_n) = \Delta\, \eta(i\sqrt{\omega_n^2+\Delta^2}), \quad (29)$$

η being the same function defined in Eq. (27). The two above equations express an important physical property, namely, that nonmagnetic disorder is a non-pair-breaking perturbation in a BCS superconductor. Indeed Eqs. (28) and (29) imply a perfect cancellation in the s-wave Cooper channel between the wave-function renormalization (the self-energy) and the vertex corrections brought by the impurities. This leads to the well-known "Anderson theorem,"[42] stating that the value of T_c is independent of the concentration of nonmagnetic impurities, provided the latter is low. This result follows immediately from the BCS gap equation in the presence of an attractive coupling[41] λ,

$$1 = \lambda T \sum_{i\omega_n} \sum_{\mathbf{k}} \frac{\eta(i\sqrt{\omega_n^2+\Delta^2})}{(\omega_n^2+\Delta^2)\,\eta(i\sqrt{\omega_n^2+\Delta^2}) + \epsilon_{\mathbf{k}}^2}. \quad (30)$$

T_c is determined by solving (30) with $\Delta=0$, namely, $\eta(i\omega_n) = 1 + 1/(2\tau|\omega_n|)$. One readily realizes that, summing over momentum first, $\eta(i\omega_n)$ disappears from the equation in the infinite-bandwidth limit, leading to the same logarithmically singular sum over Matsubara frequencies as in the absence of disorder.

We discussed previously that the emergence of SCS can be explained by assuming that vertex corrections compensate exactly for the strong wave-function renormalization. It is then tempting to further pursue the analogy with dirty s-wave superconductors. That is, we define

$$i\omega_n - \Sigma_{11}(i\omega_n) \equiv \frac{i\omega_n}{Z(i\omega_n)}, \tag{31}$$

where $\Sigma_{11}(i\omega_n)$ is the self-energy of the metastable normal solution, using instead of $\eta(i\omega_n)$ the more conventional notation $Z(i\omega_n)$ for the frequency-dependent wave-function renormalization. We then assume that allowing for superconductivity leads to diagonal, Σ_{11}, and off-diagonal, Σ_{12}, self-energy matrix elements, in the Nambu-spinor notation, given as in (28) and (29) by

$$i\omega_n - \Sigma_{11}(i\omega_n) = \frac{i\omega_n}{Z(i\sqrt{\omega_n^2 + \Delta^2})}, \tag{32}$$

$$\Sigma_{12}(i\omega_n) = \frac{\Delta}{Z(i\sqrt{\omega_n^2 + \Delta^2})}, \tag{33}$$

where Δ is the cutoff scale introduced by superconductivity. It follows immediately that the introduction of Δ restores a conventional Fermi-liquid behavior, $\Sigma_{11} \sim -i\omega_n$, not only when $T_- = 0$ and $Z(i\omega_n) \sim |\omega_n|$, but also in the pseudogap regime where $Z(i\omega_n) \sim |\omega_n|^2$. Within this picture, superconductivity regularizes the low-frequency behavior of the normal-state self-energy both at the critical point, which is actually avoided by the onset of symmetry breaking, and in the pseudogapped phase whose singularity is cut off by Δ. As a consequence of such regularization, the low-energy pseudogap in the spectral function should change within the superconducting phase into rather sharp quasiparticle peaks at the edge of the gap, which finally disappears as the Mott insulator is approached.

Unfortunately a thorough comparison of numerical DMFT data with (32) and (33) is a very hard task, because the phenomena we want to observe involve the extremely small-frequency range (where the Fermi-liquid behavior would be recovered), which is really hard to study with present impurity solvers. For this reason, since the idea we propose is quite general, we have decided to verify the validity of our ansatz for the impurity model without self-consistency, postponing some selected DMFT comparison to the end of the section.

An important difference is that no spontaneous symmetry breaking is possible for the impurity model without self-consistency. Therefore, in order to check the validity of (32) and (33), one has to add explicitly a symmetry-breaking perturbation to the Hamiltonian (13). In Refs. 35 and 36 the impurity model

$$\mathcal{H} = -\sum_{\mathbf{k}} \sum_{a=1}^{2} \sum_{\sigma} \epsilon_{\mathbf{k}} c^{\dagger}_{\mathbf{k},a\sigma} c_{\mathbf{k},a\sigma} + (V_{\mathbf{k}} c^{\dagger}_{\mathbf{k},a\sigma} d_{a\sigma} + \text{H.c.}) - t_{\perp} \sum_{\sigma} (d^{\dagger}_{1\sigma} d_{2\sigma} + \text{H.c.}) \tag{34}$$

was considered with $U=8$, $t_\perp = 0.05$, and different Γ's, in units of half the conduction bandwidth. In this model the role of the hybridization $t_\perp$ is twofold. On one hand it generates an exchange $J_\perp = 4t_\perp^2/U$ able to drive the model through the critical point. At the same time, $t_\perp$ breaks the O(2) orbital symmetry, turning the quantum phase transition into a cross-

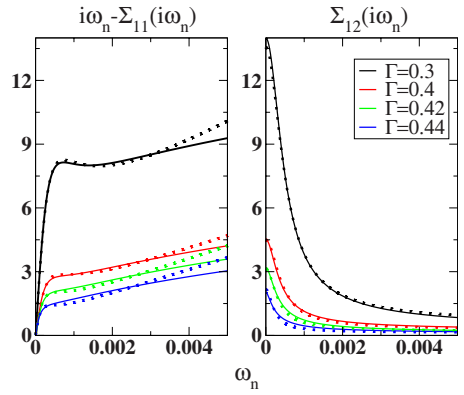

FIG. 8. (Color online) Fit of the impurity diagonal and off-diagonal self-energy, in the Nambu-spinor space, with the expressions Eqs. (32) and (33).

over which has been shown to be quite sharp.[35,36] We note that, at particle-hole symmetry, the two channels (4) and (18) are perfectly equivalent, being related by the particle-hole transformation

$$d_{2\uparrow} \to d^{\dagger}_{2\downarrow}, \quad d_{2\downarrow} \to -d^{\dagger}_{2\uparrow}, \tag{35}$$

$$c_{\mathbf{k}2\uparrow} \to -c^{\dagger}_{\mathbf{k}_*2\downarrow}, \quad c_{\mathbf{k}2\downarrow} \to c^{\dagger}_{\mathbf{k}_*2\uparrow}, \tag{36}$$

where $\mathbf{k}$ and $\mathbf{k}_*$ are particle-hole partners, $\epsilon_{\mathbf{k}} = -\epsilon_{\mathbf{k}_*}$, and $V_{\mathbf{k}_*} = V^*_{\mathbf{k}}$. Therefore we can simply borrow the NRG data of Refs. 35 and 36 and adapt them to our case of a superconducting symmetry-breaking term. In Fig. 8 we show the NRG data against our fit using Eqs. (32) and (33) with the normal self-energy that follows from the model DOS (16). The fitting parameters T_+, T_-, and Δ are shown as functions of Γ in Fig. 9.[43] We take the validity of Eqs. (32) and (33) for the impurity model as a strong support of their validity also in the lattice model even deep inside the pseudogap phase where, as previously mentioned, our numerical data have not enough precision to reveal the very low-frequency structure. An interesting feature of the off-diagonal self-energy in the impurity model is the strong frequency dependence, espe-

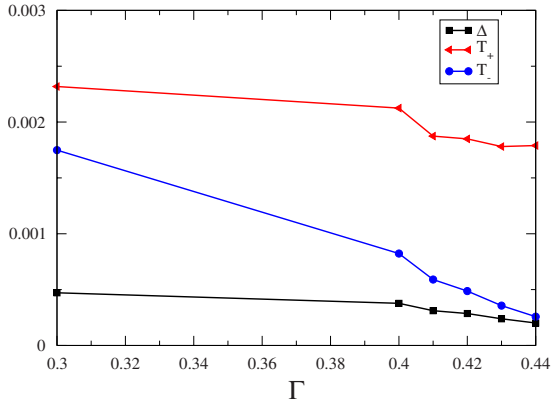

FIG. 9. (Color online) Fitting parameters T_+, T_-, and Δ of the impurity-model self-energy with the ansatz Eqs. (32) and (33) as a function of the hybridization Γ.

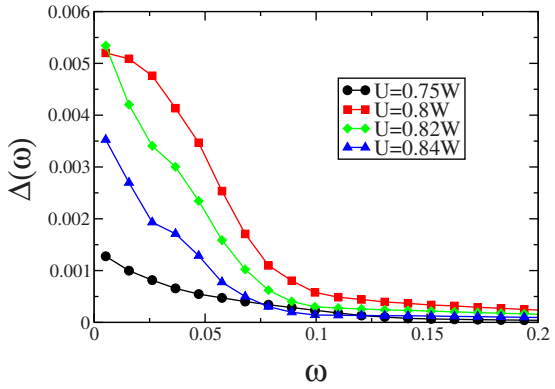

FIG. 10. (Color online) Frequency-dependent superconducting gap for several values of U.

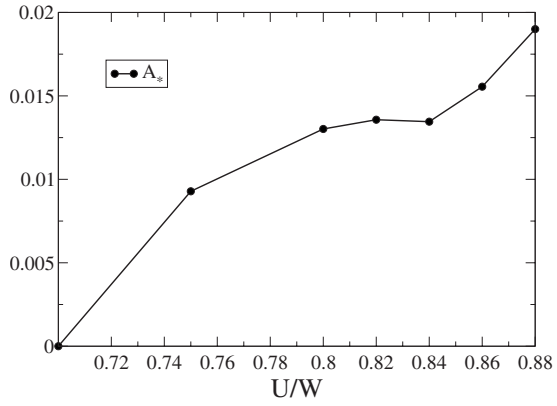

FIG. 11. Attractive coupling constant A_* extracted through Eq. (30) as the value that gives the correct DMFT value of Δ.

cially in the pseudogap region, where Σ_{12} is extremely peaked at very low frequencies. This is true also in the actual DMFT calculation. In Fig. 10 we plot, for different U's around the top of the SCS region, $U \simeq 0.82\ W$, the frequency-dependent superconducting gap, defined by

$$\Delta(i\omega_n) = \frac{i\omega_n \underset{12}{\Sigma}(i\omega_n)}{i\omega_n - \underset{11}{\Sigma}(i\omega_n)}, \tag{37}$$

whose zero-frequency extrapolation is the gap shown in Fig. 3. We note the rapid rise of $\Delta(i\omega_n)$ below a frequency of order T_+, confirming our prediction that, around its maximum, the gap is controlled by a single energy scale, T_+. Therefore, even though the attraction J is instantaneous, strong retardation effects develop to avoid the large repulsion U and stabilize superconductivity. It is just this strong frequency dependence of the superconducting gap (37) that marks the difference between a conventional Bose-Einstein condensation of preformed local pairs and our SCS phase, where pairs are highly nonlocal in time; see Fig. 10. We also note that a characteristic energy scale shows up in the dynamical gap function even if our model does not involve any exchange of bosons with a typical energy scale (at least not in an obvious way), as has been instead proposed for the two-dimensional Hubbard model.[44]

Finally, we conclude this section by discussing the possibility of writing down a gap equation like Eq. (30) for our model in the SCS phase, which remains an open and suggestive issue. Starting from the Fermi-liquid side, our DMFT results seem to suggest that pairing essentially involves only the strongly renormalized quasiparticles. In this case a natural candidate for a gap equation would be

$$\Delta = A_* T \sum_n \sum_{\mathbf{k}} F_{qp}(i\omega_n, \mathbf{k}), \tag{38}$$

where A_* is the renormalized scattering amplitude in the Cooper channel defined through Eq. (12) while F_{qp} is the quasiparticle anomalous Green's function,

$$F_{\mathrm{qp}} = \frac{1}{Z} F(i\omega_n, \epsilon_{\mathbf{k}}). \tag{39}$$

A first analysis shows that Eq. (38) correctly reproduces the order of magnitude of Δ also in the strongly correlated regime. This encourages us to use it to estimate the effective attraction A_* such that Eq. (38) gives the actual DMFT value of Δ. We use (38) and (39) also in the pseudogap state, where the Fermi-liquid ansatz for A_*, Eq. (12), is not valid. Here Z is taken to be the low-energy spectral weight within a window of the order $4J$ around the Fermi level. A_* that we obtain in this way, shown in Fig. 11, is quite smooth as a function of U and it stays relatively small, in the range between 0.01 and 0.02, up to the Mott transition. This shows that, even in the pseudogap regime, Eq. (38) can be satisfied without requiring a big coupling constant.

VII. DISCUSSION AND CONCLUSIONS

It is common wisdom that the emergence of local moments out of the incipient Mott localization must necessarily lead to an enhanced magnetic response and eventually to a magnetic order that may appear already in the metallic phase adjacent to the Mott insulator. It is equally conceivable that, under these circumstances, a system may become easily unstable to lattice distortions. Moreover, on the brink of charge localization, the orbital momentum also, quenched by the hopping deep in the metallic phase, may reemerge, making spin-orbit coupling effective as if the atoms were isolated. This is the typical phenomenology of magnetic Mott insulators exemplified by the prototype Mott-Hubbard system, V_2O_3.[45,46] These properties can be interpreted within a Landau Fermi-liquid framework only by invoking an almost perfect cancellation between the large wave-function renormalization associated with the Mott transition and the vertex corrections in particular channels. Physical intuition suggests that such channels should be primarily those acting on degrees of freedom orthogonal to charge, like spin and orbital momentum.

However, while the above arguments are quite natural, if not obvious, for particle-hole instabilities like magnetism, they sound much less trivial in connection with supercon-

ducting particle-particle instabilities. The main difference is that superconductivity implies phase coherence, which cannot survive charge localization. Nevertheless, while phase coherence requires pairing, the opposite is not true, since a Mott insulator can be formed by incoherent pairs. An example is a valence-bond crystal formed by an ordered array of tightly bound singlets on nearest-neighbor bonds, and, seemingly, also a Mott insulator made of resonating valence bonds—the RVB scenario originally proposed by Anderson[16] for high-T_c superconductors.

Another possibility is to form local singlets by exploiting the orbital degrees of freedom, which play a role similar to the bonds of the previous examples. This is realized in our model (1), and in the model for fullerenes. In the fullerene family, tetravalent alkali-metal-doped C_{60} may be regarded as the parent Mott insulating compound[22,23] that turns superconducting upon doping, the trivalent materials. The former compounds are indeed nonmagnetic Mott insulators where the four electrons occupying the LUMO of each molecule bind into a nondegenerate spin-singlet configuration because of the Jahn-Teller effect.[47]

In all these examples, the pairing implicit in the Mott state is perfectly compatible with strong repulsion; hence it is not surprising that, on moving away from the Mott insulator, superconductivity appears. The general conditions are elucidated by our analysis: pairing must correlate degrees of freedom orthogonal to charge. For instance, in the t-J model for cuprates, pairing is provided by spin superexchange, which is unaffected by the strong-repulsion constraint of no double occupancy, while it competes with hopping. The former favors configurations in which two singly occupied nearest-neighbor sites are bound into a singlet state, while the latter prefers a democratic occupancy, in which the singlet is equally as probable as any of the triplet states. Also, in our two-orbital model (1) close to the Mott transition, J competes with hopping rather than U. At half filling the hopping favors an equal occupation of all the states with two electrons per site, while J breaks this degeneracy in favor of the singlet configuration (5). Just the same competition emerges in the impurity model (13) between the Kondo temperature and J. The reason that $J \ll t$ eventually prevails in all the above examples is that the hopping suffers from a very severe wave-function renormalization close to a Mott transition, while J does not.

From these observations it appears evident that the physics of our model (1) and that of the t-J model for cuprates within the RVB scenario[14,16,19,20] share common features; our inverted exchange playing on site a similar role as the nearest-neighbor exchange in the t-J model. Quite obviously J being on site or on a link is expected to introduce relevant differences as far as the momentum structure is concerned (the most evident being s-wave versus d-wave pairing). There are, however, other relevant differences, at least regarding the interpretation of the various phases, In the RVB scenario uncovered by slave-boson[14,19,20,48] and variational[49–53] approaches, a lot of emphasis is placed on the pseudogap regime close to the Mott transition to explain superconductivity.[14] In our model, superconductivity is instead the low-temperature response to the instability in the crossover region between the pseudogap and the Fermi liquid. Another important difference is that our pseudogap state is a stable thermodynamic phase with zero entropy at zero temperature, while in the RVB scenario it appears as a fluctuating mixture of competing orders, unable to survive down to zero temperature.

Our results also look different from those of QCP theories for the cuprates.[8–10] Within the QCP approach, superconductivity arises because of the critical fluctuations around a true quantum critical point that separates stable zero-temperature phases. This critical point may even be inaccessible in the physical space of parameters, and exist only in a hypothetical enlarged space, yet it is believed to influence the physical system not only at finite but also down to zero temperature. In contrast, in model (1) the normal Fermi-liquid metal, the pseudogap phase, the superconductor and other possible symmetry-broken phases are all equally legitimate outcomes of an underlying competition that reveals itself only in the high-temperature non-Fermi-liquid crossover region, NFL in Fig. 7. From this point of view, the difference between the phase diagram Fig. 7 and the QCP scenario is the same one emphasized recently by Anderson.[54] An obvious and pertinent criticism of our claim is that, upon applying a sufficiently high magnetic field able to completely wash out superconductivity, the unstable critical region should move down to zero temperature and transform into a true quantum critical point, thus recovering the QCP scenario. We note, however, that, at its maximum, the superconducting gap is controlled only by the energy scale T_+, which is also the bandwidth of the low-energy incoherent excitations. For this reason we believe, although we cannot prove it, that a magnetic field so strong as to completely suppress superconductivity would drive the model into a phase with very poor lattice coherence, rather than revealing the critical point.

We believe that our results provide a different perspective about the relation between a pseudogap and superconductivity, which crucially differs from previous approaches. Rather than being in competition, the pseudogap and the superconducting gap turn out to be much more "compatible" with one another than in most theoretical approaches that we are aware of. A central aspect, discussed in Sec. VI, is that the large normal self-energy responsible for the pseudogap state is regularized by the onset of superconductivity, in contrast with approaches in which the same (highly anomalous) normal self-energy is assumed in the normal and superconducting states.[55] Moreover, we have shown that in model (1) there is no need for a large coupling constant to overcome the lack of low-energy density of states in the normal phase, as happens instead in approaches where pairing takes place starting from a normal state with mean-field-like pseudogaps.[56,57]

Another important outcome of our calculation is the natural appearance of two energy gaps with different behaviors as a function of the distance from the Mott insulator (see Fig. 1): the pseudogap scale T_- increases on approaching the Mott state, where it is largest, while the superconducting coherence scale vanishes as the Mott insulator is approached. This is clearly reminiscent of the two energy scales (gaps) observed in the cuprates.[58,59]

Finally, we want to emphasize that the physics we have unraveled seems to be more general than the specific toy

model (1). Indeed, we have shown that the emergence of a reinforced superconductivity upon approaching the Mott transition can be explained in the model (1) by simple Fermi-liquid arguments that do not depend on the specific model. They simply state that any scattering channel involving degrees of freedom orthogonal to charge should strengthen near a Mott transition, irrespective of whether it is a particle-particle or a particle-hole channel. This is obvious, for instance, in one dimension because of the dynamical separation of the charge from the other degrees of freedom, and explains why the phase diagram of (1) in one dimension does not differ qualitatively from Fig. 7.[28] In addition, the impurity-model analogy, which we have exploited in this work, indicates that some kind of pseudogap phase—the bulk counterpart of an impurity unscreened regime—might be ubiquitous near a Mott transition, especially if this transition is continuous. Indeed, it is obvious that a metal should suppress spectral weight around the chemical potential to smoothly connect to a realistic zero-entropy insulator, and, in the absence of symmetry breaking, we do not see any other way but opening a pseudogap. This would in turn imply also the existence of a high-temperature crossover regime that separates the Fermi-liquid phase from the pseudogap one and actually contains the seeds of the symmetry-broken phase that eventually emerges at low temperature.[36] However, it often happens that the Mott transition is first order, in particular when accompanied by a lattice distortion, as in V_2O_3.[45] In this case both the pseudogap and the critical crossover regions might become inaccessible and a discontinuous transition might occur directly from the Fermi-liquid metal to the Mott insulator.

ACKNOWLEDGMENT

We are grateful to Lorenzo De Leo for providing us with his numerical renormalization group data on the impurity model.

[1] C. A. R. Sá de Melo, M. Randeria, and J. R. Engelbrecht, Phys. Rev. Lett. **71**, 3202 (1993).
[2] R. Haussmann, Z. Phys. B: Condens. Matter **91**, 291 (1993).
[3] N. Andrenacci, A. Perali, P. Pieri, and G. C. Strinati, Phys. Rev. B **60**, 12410 (1999).
[4] B. Kyung, S. Allen, and A.-M. S. Tremblay, Phys. Rev. B **64**, 075116 (2001).
[5] A. M. Tsvelik and A. V. Chubukov, Phys. Rev. Lett. **98**, 237001 (2007) and references therein.
[6] Y. Wang, L. Li, and N. P. Ong, Phys. Rev. B **73**, 024510 (2006).
[7] A. Kanigel *et al.*, Nat. Phys. **2**, 447 (2006).
[8] C. M. Varma, Phys. Rev. B **55**, 14554 (1997).
[9] C. Castellani, C. Di Castro, and M. Grilli, Z. Phys. B: Condens. Matter **103**, 137 (1997).
[10] J. L. Tallon and J. W. Loram, Physica C **349**, 53 (2001).
[11] A. J. Millis, Phys. Rev. B **48**, 7183 (1993).
[12] P. Coleman, C. Pepin, Q. Si, and R. Ramazashvili, J. Phys.: Condens. Matter **13**, R723 (2001).
[13] Q. Si, Adv. Solid State Phys. **44**, 253 (2004).
[14] P. A. Lee, N. Nagaosa, and X.-G. Wen, Rev. Mod. Phys. **78**, 17 (2006), and references therein.
[15] S.-C. Zhang, Science **275**, 1089 (1997).
[16] P. W. Anderson, Science **235**, 1196 (1987).
[17] A. Georges, G. Kotliar, W. Krauth, and M. J. Rozenberg, Rev. Mod. Phys. **68**, 13 (1996).
[18] M. Capone, M. Fabrizio, C. Castellani, and E. Tosatti, Phys. Rev. Lett. **93**, 047001 (2004).
[19] G. Kotliar and J. Liu, Phys. Rev. B **38**, 5142 (1988).
[20] Y. Suzumura, Y. Hasegawa, and H. Fukuyama, J. Phys. Soc. Jpn. **57**, 2768 (1988).
[21] O. Gunnarsson, Rev. Mod. Phys. **69**, 575 (1997).
[22] M. Capone, M. Fabrizio, and E. Tosatti, Phys. Rev. Lett. **86**, 5361 (2001).
[23] M. Capone, M. Fabrizio, C. Castellani, and E. Tosatti, Science **296**, 2364 (2002).
[24] E. Plekhanov, S. Sorella, and M. Fabrizio, Phys. Rev. Lett. **90**, 187004 (2003).
[25] R. Assaraf, P. Azaria, E. Boulat, M. Caffarel, and P. Lecheminant, Phys. Rev. Lett. **93**, 016407 (2004).
[26] F. F. Assaad, Phys. Rev. B **71**, 075103 (2005).
[27] A. Paramekanti and J. B. Marston, J. Phys.: Condens. Matter **19**, 125215 (2007).
[28] M. Fabrizio and E. Tosatti, Phys. Rev. Lett. **94**, 106403 (2005).
[29] M. Caffarel and W. Krauth, Phys. Rev. Lett. **72**, 1545 (1994).
[30] M. Capone, M. Civelli, S. S. Kancharla, C. Castellani, and G. Kotliar, Phys. Rev. B **69**, 195105 (2004).
[31] W. Metzner and D. Vollhardt, Phys. Rev. Lett. **59**, 121 (1987).
[32] R. Micnas, J. Ranninger, and S. Robaszkiewicz, Rev. Mod. Phys. **62**, 113 (1990).
[33] A. Toschi, M. Capone, and C. Castellani, Phys. Rev. B **72**, 235118 (2005).
[34] M. Fabrizio, A. F. Ho, L. De Leo, and G. E. Santoro, Phys. Rev. Lett. **91**, 246402 (2003).
[35] L. De Leo and M. Fabrizio, Phys. Rev. B **69**, 245114 (2004).
[36] M. Ferrero, L. De Leo, P. Lecheminant, and M. Fabrizio, J. Phys.: Condens. Matter **19**, 433201 (2007).
[37] H. R. Krishna-murthy, J. W. Wilkins, and K. G. Wilson, Phys. Rev. B **21**, 1003 (1980).
[38] H. R. Krishna-murthy, J. W. Wilkins, and K. G. Wilson, Phys. Rev. B **21**, 1044 (1980).
[39] B. A. Jones and C. M. Varma, Phys. Rev. B **40**, 324 (1989).
[40] I. Affleck, A. W. W. Ludwig, and B. A. Jones, Phys. Rev. B **52**, 9528 (1995).
[41] A. A. Abrikosov, L. P. Gor'kov, and I. E. Dzyaloshinski, *Methods of Quantum Field Theory in Statistical Physics* (Dover, New York, 1963).
[42] P. W. Anderson, J. Phys. Chem. Solids **11**, 26 (1959).
[43] Since the impurity model explicitly contains the symmetry-breaking term, the self-energy that we fitted is actually the off-diagonal component of the inverse Green's function.
[44] A. Macridin, M. Jarrell, T. Maier, and D. J. Scalapino, Phys. Rev. Lett. **99**, 237001 (2007).

[45] W. Bao, C. Broholm, G. Aeppli, S. A. Carter, P. Dai, T. F. Rosenbaum, J. M. Honig, P. Metcalf, and S. F. Trevino, Phys. Rev. B **58**, 12727 (1998), and references therein.
[46] L. Paolasini *et al.*, Phys. Rev. Lett. **82**, 4719 (1999).
[47] M. Fabrizio and E. Tosatti, Phys. Rev. B **55**, 13465 (1997).
[48] G. Baskaran, Z. Zou, and P. W. Anderson, Solid State Commun. **63** (1987).
[49] C. Gros, Phys. Rev. B **38**, 931 (1988).
[50] S. Sorella, G. B. Martins, F. Becca, C. Gazza, L. Capriotti, A. Parola, and E. Dagotto, Phys. Rev. Lett. **88**, 117002 (2002).
[51] A. Paramekanti, M. Randeria, and N. Trivedi, Phys. Rev. Lett. **87**, 217002 (2001).
[52] P. W. Anderson, P. A. Lee, M. Randeria, T. M. Rice, N. Trivedi, and F. C. Zhang, J. Phys.: Condens. Matter **16**, R755 (2004).
[53] D. A. Ivanov and P. A. Lee, Phys. Rev. B **68**, 132501 (2003).
[54] P. W. Anderson, Physica B **318**, 28 (2002).
[55] K.-Y. Yang, T. M. Rice, and F.-C. Zhang, Phys. Rev. B **73**, 174501 (2006).
[56] P. Nozières and F. Pistolesi, Eur. Phys. J. B **10**, 649 (1999).
[57] L. Benfatto, S. Caprara, and C. D. Castro, Eur. Phys. J. B **17**, 95 (2000).
[58] M. Le Tacon, A. Sacuto, A. Georges, G. Kotliar, Y. Gallais, D. Colson, and A. Forget, Nat. Phys. **2**, 537 (2006).
[59] K. Tanaka *et al.*, Science **314**, 1910 (2006).